Inorganic Chemistry

Article

pubs.acs.org/IC

$Au_{10}Mo_4Zn_{89}$: A Fully Ordered Complex Intermetallic Compound Analyzed by TOPOS

Partha P. Jana,*[,†] Arina A. Pankova,[‡] and Sven Lidin[†]

[†]CAS Chemical Centre, Lund University, Getingevägen 60, Box 124, SE-22100 Lund, Sweden

[‡]Samara Center for Theoretical Materials Science (SCTMS), Samara State University, Ac. Pavlov St. 1, Samara, Russia 443011

Supporting Information

ABSTRACT: The compound $Au_{10}Mo_4Zn_{89}$ has been synthesized, and its structure has been analyzed by single-crystal X-ray diffraction. The compound crystallizes in cubic space group $F\bar{4}3m$ (No. 216) with a unit cell that contains 412 atoms. The structure is largely tetrahedrally closely packed, but an octahedral arrangement of atoms is incompatible with tetrahedral close packing. The structure of the ordered $Au_{10}Mo_4Zn_{89}$ compound has been described by using the algorithm of automatic geometric and topological analysis that is implemented in TOPOS as the "Nanoclustering" procedure.

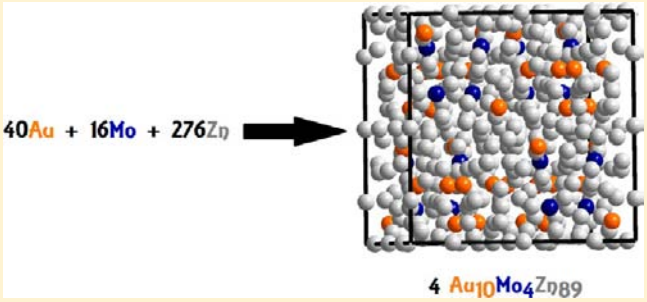

INTRODUCTION

The γ-phase occurring at approximately 21/13 (e/a) is commonly considered the structurally most complex Hume–Rothery phase in brass-like systems.[1−5] The archetype of γ-brass is Cu_5Zn_8;[5−7] however, the number of systems that exhibit γ-brass-type phases is large, and there are several recent reports on such systems.[8−11] The γ-brass-type structures crystallize in space group $I\bar{4}3m$ with a lattice parameter a of ≈9.00 Å and contain ∼52 atoms in their unit cell.

Several variations and modifications of γ- and γ-related structures are known.[11−19] Among them, the $2a \times 2a \times 2a$ superstructures of γ-brass-type or related phases are known as cubic giant cell structures.[20,21] Quite a lot of binary superstructures of γ- and γ-related phases and only a few ternary or pseudobinary systems have been studied in depth in recent years.[22−31] The γ-brass-related structures generally contain many imperfections and show several configurational disorders that are typical for structurally complex intermetallic alloys. Moreover, the structures of binary γ-brass-related phases probably offer the best possibilities of avoiding the occupational disorder that usually occurs in multicomponent γ-brass-related superstructures. A recent report revealed that the substitution of heavy transition elements into those disordered alloys may induce ordering.[31,32] For instance, the γ-brass-related binary $CrZn_{17}$ is heavily disordered, exhibiting a complex interplay of occupational and displacive disorder; but, upon addition of Au, the degree of disorder decreases gradually with the substitution of Cr and Zn for Au, and at the limiting composition, $Au_{10}Cr_4Zn_{89}$, the structure is fully ordered. It has been also shown that the phase is controlled by the Hume–Rothery stabilization rule. The exchange of Zn and Cr for Au leads to a close to ideal VEC (e/a). The previous work on Au–Cr–Zn ternary complex metallic alloys inspired us to dope Au into the $MoZn_{20.44}$[23] disordered binary intermetallic alloy. The structure of $MoZn_{20.44}$ is roughly isopointal to that of congeneric $CrZn_{17}$, although the atomic decoration and hence the occupational and positional disorder are distinct in the two compounds. In the Au–Cr–Zn ternary system, it was no easy task to differentiate the site preference between Cr and Zn by X-ray diffraction data because of the weak scattering contrast. A reliable chemical composition of individual sites could only be determined by a combination of X-ray single-crystal refinement, electronic structure calculations, and EDS compositional analysis. The investigation of the Mo-based system has an advantage in that Mo has strong scattering contrast compared to that of gold and zinc. This fact may permit us to distinguish the atomic site of Mo uniquely by the result of the X-ray diffraction experiment.

This motivated us to synthesize $Au_{10}Mo_4Zn_{89}$ in the hope of finding a new ternary ordered phase in the Au–Mo–Zn system according to the following scheme:

$$10Au + 4Mo + 89Zn \Rightarrow Au_{10}Mo_4Zn_{89}$$

In this report, we will discuss the existence, and structural features, and report on preliminary electronic structure investigations of the new, ordered γ-brass-related compound $Au_{10}Mo_4Zn_{89}$ discovered in this Au–Mo–Zn ternary system.

EXPERIMENTAL SECTION

Syntheses. The $Au_{10}Mo_4Zn_{89}$ compound was synthesized by a high-temperature reaction starting from the pure constituent elements: Au (99.995%, Aldrich), Mo (99.995%, Aldrich), and Zn (99.9999%, Chempur). Samples of precisely weighed metals (approximately 0.3 g each) were loaded and sealed in argon-purged evacuated silica ampules (3 cm in length and 0.8 cm in diameter). The target phase was synthesized using an electric muffle furnace. The metal mixture was

Received: May 28, 2013
Published: September 13, 2013

   dx.doi.org/10.1021/ic4013312 | *Inorg. Chem.* 2013, 52, 11110−11117

heated at a rate of 194.4 K/h to 1273 K, a temperature at which the ampules were kept for 2 h. Hereafter, the temperature was reduced to 703 K at a rate of 114 K/h, and the sample was annealed at this temperature for 5 days. Subsequently, the samples were either quenched in cold water or cooled to ambient temperature. Products obtained from these reactions were silvery, brittle ingots and were found to be stable in air.

X-ray Diffraction Data Collection and Processing. After the sample tube had been broken, the resulting ingots of the ternary $Au_{10}Mo_4Zn_{89}$ compound were crushed, suitable crystals (C1 and C2) were picked and mounted on a glass fiber, and diffraction intensities were measured with an Oxford Diffraction XCalibur Eos instrument equipped with Mo Kα radiation (λ = 0.71073 Å, 50 kV, 40 mA) at ambient temperature. Data collection and reduction were performed with the Oxford diffraction Crysalis system. The diffraction patterns could conclusively be indexed on the basis of an ~18 Å F-centered cubic unit cell. The structure solution and the refinement were conducted using Jana2006.[33,34] Crystallographic information about C1 is listed in Table 1. Details of the crystallographic information about C2 can be obtained from the Supporting Information.

Energy Dispersive X-ray Analysis. The composition of the selected specimens were examined in a scanning electron microscope [JEOL 3000 with a secondary electron (SEI) detector] with an energy dispersive X-ray spectrometer (EDS). Energy dispersive X-ray spectra were recorded from the samples that had been studied by single-crystal X-ray diffraction. No impurities heavier than carbon were detected in the selected samples.

Table 1. Crystallographic Data for the Single-Crystal Structure Refinements of $Au_{10}Mo_4Zn_{89}$(C1)

chemical formula	$Au_{10}Mo_4Zn_{89}$
EDS formula	$Au_{9.8}Mo_{4.3}Zn_{88.9}$
Pearson symbol	*cF*412
mole fraction of gold (x_{Au})	0.0970
crystal system	cubic
space group type; Z	$F\bar{4}3m$ (No. 216); 4
a (Å)	18.5878(3)
V (Å^3)	6422.23(18)
ρ_{calcd} (Mg/m^3)	8.4494
μ (mm^{-1})	55.965
crystal color	silvery with a metallic luster
Data Collection	
diffractometer	four-circle diffractometer, Xcalibur, Eos
radiation	Mo Kα
monochromator	graphite
crystal−IP distance (mm)	45
T (K)	293(2)
$2\theta_{max}$ (deg)	52.64
no. of measured reflections	3403
index range	$-23 \le h \le 23$
	$-17 \le k \le 10$
	$-25 \le l \le 24$
completeness of data set	0.9923
absorption correction	multiscan
no. of unique reflections	665
R_{int}	0.0554
structure determination/refinement	*JANA* 2006 package program[33]
structure determination	Superflip[34]
no. of reflections used	665
no. of variables	63
no. of observed reflections [$I > 3\sigma(I)$]	535
R [$F^2 > 3\sigma(F^2)$]	0.0328
$R(F)$ (all data)	0.0473
k^a	0.0004
wR (F^2) (all data)	0.0654
GOF (all)	1.08
$\Delta\rho_{min}/\rho_{max}$ (e Å^{-3})	−2.62/3.31

[a]weighting scheme: w =1/[σ^2(I)+k(I)^2)].

Details of the Description by TOPOS. Given the excellent X-ray contrast among the three constituent metals (Au, Mo, and Zn), we felt confident that the refined composition reflected perfect ordering, and this prompted a more detailed analysis of the structure. In particular, very few perfectly ordered 2 × 2 × 2 γ-brass superstructures are known.[26] Thus, we extend the analysis of the structure by using the algorithm of automatic geometric and topological analysis that is implemented in TOPOS as the "Nanoclustering" procedure, applicable for any intermetallic compound.[35,36]

(i) The crystal structure is formed by multishell primary onion-like nanoclusters, which usually contain two or three shells. The structure assembly of the primary nanoclusters predetermines the topology of the underlying net, i.e., the net of the nanocluster centers.

(ii) The centers of the primary nanoclusters occupy the most highly symmetrical positions of the structure.

(iii) The primary nanoclusters are usually centered with highly coordinated atoms. However, the nanoclusters can be "empty" (noncentered) if they obey principles i and ii.

(iv) The primary nanoclusters do not interpenetrate, i.e., have no common internal atoms, but they may share their surface atoms.

(v) In some cases, a few atoms or one-shell clusters fill voids between primary nanoclusters playing the role of spacers. The set of primary nanoclusters and spacers should include all atoms of the structure.

(vi) The primary nanoclusters condense into supraclusters which, in turn, form microchains. A successive condensation of microchains gives rise to microlayers and finally to a microframework that predetermines the topology of the underlying net.

(vii) In special cases where several inequivalent models obey principles i−vi, the additional criterion of assembling a minimal number of unique primary nanoclusters needs to be used (i.e., the parsimony principle), and finally, the number of inequivalent nodes may be minimized.

Electronic Structure Calculations. To understand the stability of the $Au_{10}Mo_4Zn_{89}$ compound from a chemical perspective, we conducted electronic structure calculations using the refined crystallographic results as a model. The tight binding, linear muffin-tin orbital (TB-LMTO) method with the atomic sphere approximation (ASA) has been used for this purpose.[37−40] Exchange and correlation were treated in the von Barth−Hedin local density approximation.[41] All relativistic effects except spin−orbit coupling were taken into account by using a scalar relativistic approximation.[42] In the ASA, space is filled with small, overlapping Wigner−Seitz (WS) spheres at each atomic site. The symmetry of the potential is considered to be spherical inside each WS sphere, and a combined correction takes into account the overlapping part. The radii of the WS spheres were obtained by requiring that the overlapping potential should give the best possible approximation to the full potential by an automatic procedure.[43] Seven empty spheres were needed to satisfy the LMTO volume criterion. The basis set included 5s, 5p, and 5d orbitals of Au; 4s and 4p orbitals of Zn; and 5s, 5p, and 4d orbitals of Mo. The Brillouin zone integrations were accomplished on an 8 × 8 × 8 k-point mesh with the tetrahedron method.[44] The curves of the density of states (DOS) and crystal orbital Hamiltonian population (COHP) were plotted.

RESULTS

Structural Determination and Refinement. The structure was solved in noncentrosymmetric space group $F\bar{4}3m$ (No. 216). Atomic positions missing in the original model were included from residual electron density maps. The structure solution and subsequent refinement yielded 15 atomic positions in the asymmetric unit: two gold sites (Au12 and Au23), one molybdenum site (Mo42), and 12 zinc sites (see Table S1 of the Supporting Information). At this stage, the structure

dx.doi.org/10.1021/ic4013312 | Inorg. Chem. 2013, 52, 11110−11117

refinement converged at $R(F) \approx 0.06$. All refined occupancy factors were reset to unity in the final refinement cycles as they deviated by less than a single standard deviation from that value. Anisotropic displacement parameters of the atoms were then introduced, and the final refinement, including an isotopic extinction correction, yields an $R(F^2)$ $[F^2 > 3\sigma(F^2)]$ value of 0.03. A refinement model taking inversion twinning into account was attempted, but the refined relative volume of the inversion twin cannot be considered significant. Details concerning the atomic coordinates, equivalent isotropic displacement parameters, and anisotropic displacement parameters are listed in Table S1 of the Supporting Information.

Chemical compositions determined by X-ray single-crystal refinements were supported by the EDS analysis (see Table 1).

Structural Characteristics. Binary $MoZn_{20.44}$ forms a complex, heavily disordered structure that can be seen as comprising structural units as in γ-brass, tungsten, α-manganese, and Ti_2Ni. Upon addition of Au to binary $MoZn_{20.44}$, a fully ordered structure is formed, having a composition of $Au_{10}Mo_4Zn_{89}$, isotypic with $Au_{10}Cr_4Zn_{89}$. As previously found in $Au_{10}Cr_4Zn_{89}$, the four constitutive "clusters" in $Au_{10}Mo_4Zn_{89}$ are located at the high symmetry points of the unit cell. We use standard notation to designate each cluster type and polyhedral cell of constituting clusters.[45−47] The decoration of the four isolated clusters in $Au_{10}Mo_4Zn_{89}$ is depicted in Figure S2 of the Supporting Information and listed in Table S2 of the Supporting Information.

All clusters discussed so far are enclosed by an exterior cuboctahedal (CO) shell. A closer inspection of the atomic arrangements in $Au_{10}Mo_4Zn_{89}$ reveals that there are further atoms similar distances from the cluster center as the CO atoms forming or complementing a further shell comprising 28 atoms. The configuration of the exterior 28-atom shell depends both on the nature of the adjacent smaller clusters and on their orientation in space. The four extended clusters are depicted in Figure 1. Some characteristics of the clusters and shells are summarized in Table 2.

Cluster Z is depicted as a γ-cluster in Figure 1a. Twelve Zn15 atoms are colored 50% gray; 12 additional Zn45 atoms (dark blue) extend the γ-cluster to the typical 38-atom quadruple of icosahedra grouped around an interior Zn12 IT (Figure 1a).[48] Twelve Zn45, 12 Zn25 (blue), and 4 Zn22 (sky blue) atoms form the outer shell representing a tetrated dodecahedron (TD), $3^{16}.5^{12}$, with an equal number of faces and vertices. Hence, we obtain a Au_4Zn_{50} (□@Zn4@Au4@Zn6@Zn12@Zn28) cluster.

Cluster Q can also be viewed as a γ-cluster in Figure 1b. The 28 ensuing atoms, 12 CO Zn35 (dark teal), 12 Zn15 (light blue), and 4 Zn32 (sky blue) atoms, form a tetrated dodecahedron (TD) confining the extended Au_6Zn_{48} (□@Zn4@Zn4@Au6@Zn12@Zn28) cluster. The composition of the extended H cluster is Mo_4Zn_{41}. The 28 outer atoms, formed by 12 Zn35 (dark teal), 12 Zn25 (sky blue), and 4 Mo42 (red) atoms, cap the 28 triangulated faces of the interior deltahedral Zn_{17} unit (Frank−Kasper polyhedral)[49] as emphasized by the 50% gray color (Figure 1c). Hence, the outer shell is the dual form of the 16-vertex Frank−Kasper polyhedron (also known as the Friauf polyhedron), which is described by the polyhedral formula $5^{12}.6^4$. The principle of duality[50] holds also for the next atomic shell formed by 12 Zn45 and 4 Zn21 atoms. Consequently, the configuration of these atoms conforms to a second, enlarged self-similar Friauf polyhedron with its

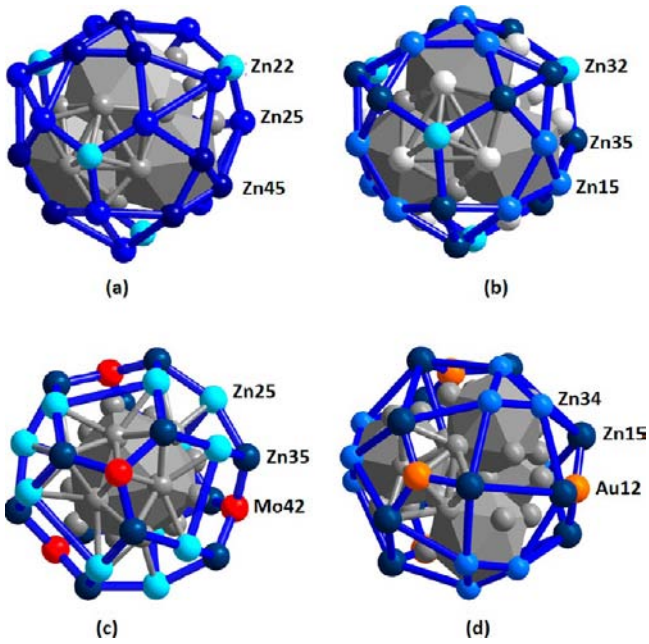

Figure 1. Representation of 28-atom polyhedra in the crystal structure of $Au_{10}Mo_4Zn_{89}$. Clusters a−d are located around high symmetry points of the unit cell: (0 0 0), ($^1/_4$ $^1/_4$ $^1/_4$), ($^1/_2$ $^1/_2$ $^1/_2$), and ($^3/_4$ $^3/_4$ $^3/_4$), respectively. Zinc atoms of 28-atom polyhedra are colored blue, molybdenum atoms red, and gold sites orange. Zinc atoms of the polyhedra described above from different sites have been recognized by the variation of the concentration of the blue color.

Table 2. Description of 28-Atom Polyhedra about Special Sites Z, Q, H, and T

cluster	subshell	vertex configuration	polyhedral formula
Z(1)	Zn22	5^3	tetrated dodecahedron
	Zn25	$5^2.3^2$	$3^{16}.5^{12}$
	Zn45	5.3.5.3	
Q(2)	Zn15	5.3.5.3	tetrated dodecahedron
	Zn35	$5^2.3^2$	$3^{16}.5^{12}$
	Zn32	5^3	
H(3)	Mo42	5^3	fullerene
	Zn25	6.5^2	$5^{12}.6^4$
	Zn35	6.5^2	
T(4)	Au12	4^3	$3^4.4^{24}$
	Zn34	4.4.4.3	
	Zn15	4.4.4.4	

vertices located above the 16 faces of the $5^{12}.6^4$ fullerene cage. The 16 additional atoms extend the 28-atom polyhedron to a 44-atom polyhedron enclosed by 84 triangles. A particular outcome of this building principle based on triangulation and duality is a clean tetrahedrally closely packed Mo_4Zn_{57}. The H cluster is composed of 28 + 28 + 24 + 60 = 140 slightly distorted, space-filling tetrahedra. The fourth Ti_2Ni-type T cluster does not stick to this principle, because an octahedral arrangement of atoms is incompatible with tetrahedral close packing. The expansion of the T cluster by 12 Zn34 atoms (light blue) imports a quadruple of icosahedra that is intensified by 50% gray color as shown in Figure 1d. The tetrahedron of vertex-sharing icosahedra resembles the "L-unit" introduced by Kreiner and Franzen.[51] Each of the four icosahedra is condensed to a triangular face of an octahedron built up by 6 Zn43 atoms. The 28-atom shell is formed by 12 Zn15 (dark

dx.doi.org/10.1021/ic4013312 | Inorg. Chem. 2013, 52, 11110−11117

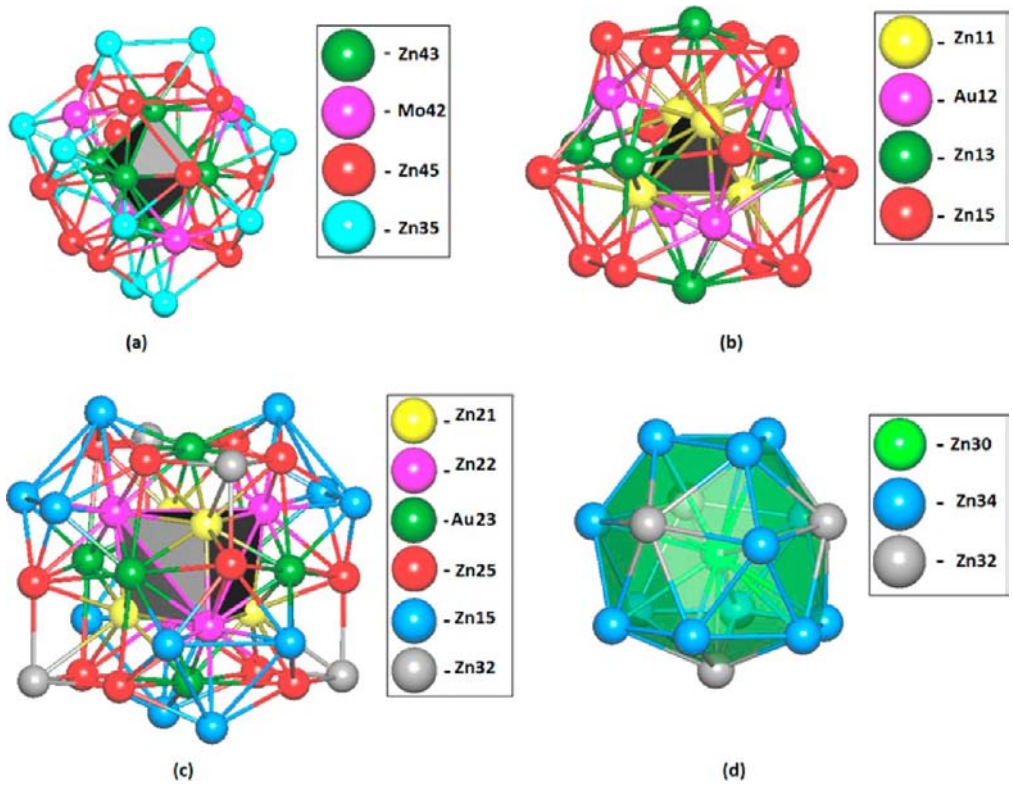

Figure 2. (a) □@6@28 primary nanoclusters based on the Ti_2Ni cluster. Twelve additional atoms of the nanoclusters that form a truncated tetrahedron are Zn35 atoms. (b) □@4@22 primary nanocluster considered as the γ-brass-type nanocluster. (c) □@8@34 primary nanocluster that includes the □@8 inner core in the form of two nested tetrahedra. The truncated tetrahedron and external tetrahedron are colored blue and gray, respectively. (d) 1@16 Friauf polyhedron that plays the role of spacer.

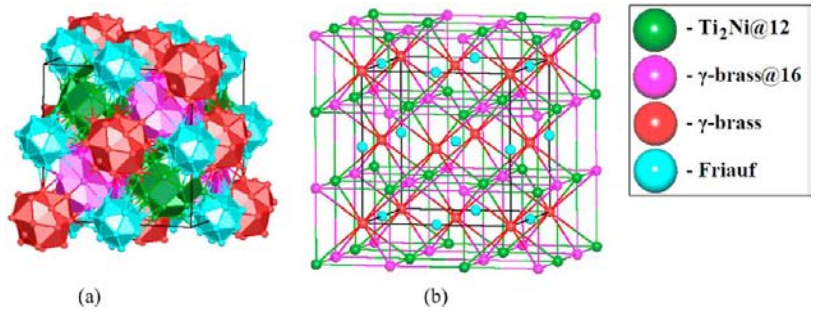

Figure 3. (a) Assembly of 34-atom (Ti_2Ni-based), 26-atom (γ-brass-type), and 42-atom (γ-brass-based) primary nanoclusters and Friauf polyhedra that form a **bcu-x** underlying net (b).

teal) and 4 Au12 (orange) atoms; 4 × 3 Zn15 atoms make a $3^4.6^4$ truncated tetrahedron (TT), and 4 × 3 Zn34 atoms are located above the 4 hexagons of the TT and 4 Au12 atoms above the triangles of the TT. Twenty-eight polygons consisting of 12 kites, 12 trapezoids, and 4 triangles form the circumference of the extended T cluster. The composition of the extended cluster is $Au_4Mo_4Zn_{54}$.

Nanocluster Description of the $Au_{10}Mo_4Zn_{89}$ Structures. Using the nanocluster approach and TOPOS, we took into account the interatomic interactions corresponding to those faces of the atomic Voronoi–Dirichlet polyhedra that have solid angles (Ω) that are 1.5% of the 4π steradian. To check the stability of the models obtained, we considered also the Ω = 5% level that resulted in some weak contacts that were ignored.

When Ω was >1.5%, we found a total of 364 models, but applying all principles of nanoclusters, we came to a few models, which are briefly described below.

The main model can be described as a □@6@28 + □@4@22 + □@8@34 + 1@16 combination of nanoclusters in positions ($^3/_4\ ^3/_4\ ^3/_4$), (0 0 0), ($^1/_4\ ^1/_4\ ^1/_4$), and ($^1/_2\ ^1/_2\ ^1/_2$), respectively. Nanocluster 0@6@28 (Figure 2a) can be considered as an analogue of the Ti_2Ni cluster with 12 additional Zn35 atoms, which form an outer truncated tetrahedron (TT). In addition, there are two types of γ-brass-type nanoclusters. The first one, □@4@22, is the classical γ-brass cluster with the inner tetrahedral core (Figure 2b). The second one, □@8@34, includes the □@8 inner core in the form of two nested tetrahedra (Figure 2c). The second shell of this cluster contains 34 atoms and can be described as a OH + CO + TT + ET sequence of nested polyhedra, where TT and ET are a truncated tetrahedron and an external tetrahedron,

dx.doi.org/10.1021/ic4013312 | Inorg. Chem. 2013, 52, 11110–11117

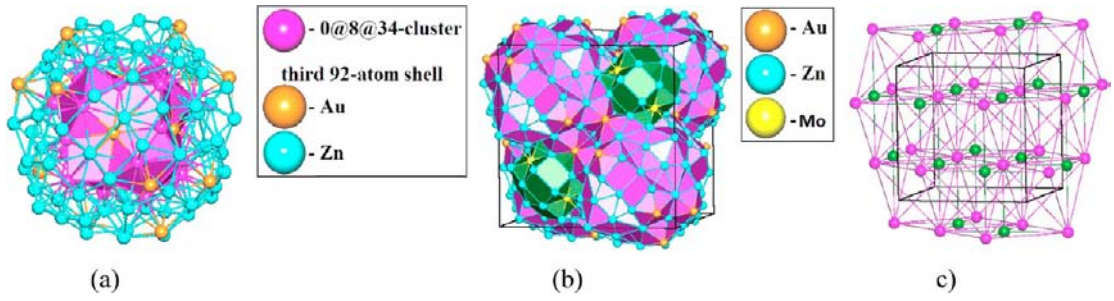

Figure 4. Alternative model of the $Au_{10}Mo_4Zn_{89}$ crystal structure represented as a combination of three-shell 0@8@34@92 primary nanoclusters (a), with the Ti_2Ni-based □@6@28 primary nanoclusters (b) that form an **ast-d** underlying net (c).

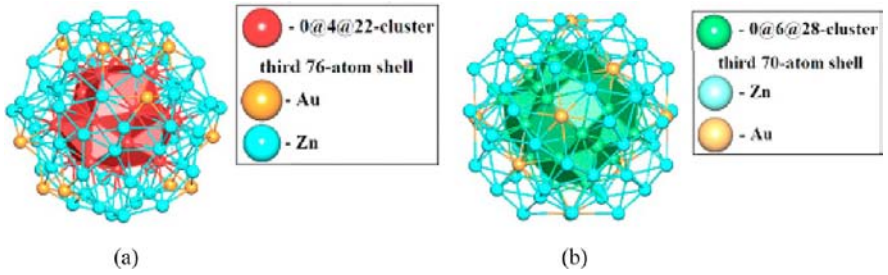

Figure 5. Three-shell □@4@22@76 (a) and □@6@28@70 (b) primary nanoclusters in the $Au_{10}Mo_4Zn_{89}$ structure.

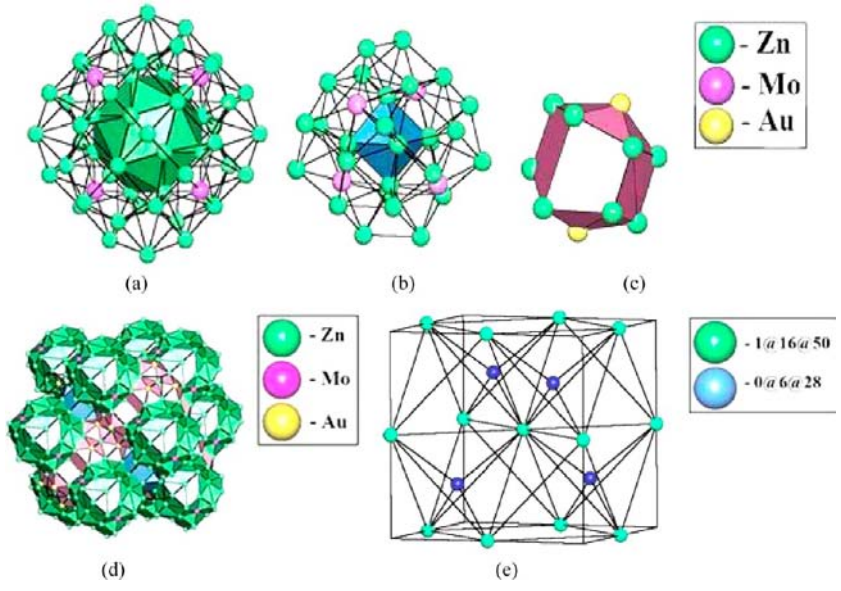

Figure 6. (a) 1@16@50 primary nanocluster based on the Friauf polyhedron. (b) □@6@28 primary nanocluster based on the Ti_2Ni cluster. (c) 1@12 polyhedron that plays the role of spacer in the $Au_{10}Mo_4Zn_{89}$ structure. (d) Assembly of the primary nanoclusters and spacers. (e) The centers of the primary nanoclusters form the **sqc349** underlying net.

respectively. Also, there is a small spacer 1@16 in the form of the Friauf polyhedron (Figure 2d). These four building units form the extended body-centered cubic net (Figure 3) that has the three-letter code **bcu-x** according to the RCSR nomenclature.[52]

Another possible model is a combination of two-shell □@6@28 and three-shell □@8@34@92 nanoclusters that occupy positions ($^3/_4$ $^3/_4$ $^3/_4$) and ($^1/_4$ $^1/_4$ $^1/_4$), respectively . As we can see, the third 92-atom shell can be grown outside the γ-brass-type clusters without interpenetration (Figure 4). There are also models with three-shell nanoclusters, □@4@22@76 and □@6@28@70, whose centers occupy the (0 0 0) and ($^3/_4$ $^3/_4$ $^3/_4$) positions, respectively (Figure 5); however, these nanoclusters combine with more than one cluster that contradicts the parsimony principle.[36]

All the models remain the same at the $\Omega > 5\%$ level, but the □@8@34 nanocluster loses four atoms of the outer shell (ET) and transforms into □@8@30.

There is also a non-γ-brass description of the $Au_{10}Mo_4Zn_{89}$ structure as a combination of the Ti_2Ni-based and Friauf-based nanoclusters and the 1@12 polyhedron playing the role of spacer (□@6@28 + 1@16@50 + 1@12). The assembly of the two-shell nanoclusters forms the binodal 3,16-coordinated **sqc349** underlying net (Figure 6).

Searching for Similarities with the Nanocluster Models. Strong evidence of the stability of nanoclusters is

dx.doi.org/10.1021/ic4013312 | *Inorg. Chem.* 2013, 52, 11110−11117

the realization of them in the structure of intermetallic compounds. In our work, we have searched for nanocluster models in atomic nets by applying the algorithm for selecting finite subgraphs in infinite periodic graphs which was realized in TOPOS. Crystal data for intermetallic compounds have been taken from ICSD (release 2011/2) and Pearson's Crystal Data (version 2010/2011). In Table 3, we present the number of structures in which 1@16, γ-brass, γ-brass@16, and Ti_2Ni@12 nanoclusters are found. Note that all of the nanoclusters that constitute the structures have maximal T_d symmetry; however, lower symmetries also occur but as local configurations. That does not adhere to the nanocluster approach. A description of the chemical composition of order structures with T_d symmetry of the 1@16, γ-brass, γ-brass@16, and Ti_2Ni@12 nanoclusters is given in Table S3 of the Supporting Information.

Table 3. Numbers of Structures Containing the Nanoclusters Found in $Au_{10}Mo_4Zn_{89}$

cluster	total no. of structures	no. of ordered structures with all nanoclusters with T_d symmetry
Friauf polyhedron (17 atoms)	3326	774
γ-brass (26 atoms)	3583	922
Ti_2Ni@12 (34 atoms)	280	89
γ-brass@16 (42 atoms)	26	6

Considering only the ordered structures with the nanocluster in T_d symmetry, we have found some common building principles. In Table 4, we list the types of chemical compositions of nanoclusters. Thus, the Friauf polyhedron can be constructed as an A@A_{16}-type, monatomic nanocluster; A@B_{16} and A@A_4B_{12}, where A is the heavier metal atom; A@B_4A_{12}, where A is the lighter metal atom; and A@B_4C_{12}, the three-component nanocluster. Structures include the Ti_2Ni@12 nanocluster that can have a pure A_6@A_{28}- or A_6@B_4A_{24}-type composition. The structures building from the γ-brass (based) nanoclusters will be considered in a separate paper[53] in detail.

Table 4. Types of Chemical Compositions of Nanoclusters

nanocluster	chemical composition of the nanoclusters	examples
Friauf	A@A16	Mn, $EuMn_{28}$, Ir_4Mg_{29}
	A@B16	$CaAu_5$, $MoBe_{22}$, EuV_2Al_{20}
	A@A4B12	ZrV_2, $ScCo_2$, $DyRh_2$
	A@B4A12	$CaAu_5$, Dy_5Mg_{24}, $Sm_{11}Cd_{45}$
	A@B4C12	$U_{17}Ni_{66}Al_{17}$, $Zr_{17}Ni_{66}In_{17}$, $CaNa_{10}Sn_{12}$
Ti2Ni@12	A6@A28	MBe_{22} (M = Mo, W, Re, Tc), MZn_{22} (M = Hf,Zr), $NdCr_2Al_{20}$, UCr_2Al_{20}
	A6@B4A24	$CeCo_2Al_{20}$, $DyRh_2Zn_{20}$, Mg_3Ti2Al_{18}
γ-brass	A4@A22	$Li_{13}Na_{29}Ba_{19}$
	A4@B22	Ce_4RuCd, $CoTi_2$, Dy_4RhCd
	A4@A4B6C12	$Al_{16}Co_7Hf_6$, $Al_7Cu_{16}Er_6$, $Be_{15}Cu_8Ta_6$
	A4@A4B18	$Hf_{1.5}Mn_{1.5}$, NiCd
	A4@A6B4C12	$Be_{15}Cu_8Ta_6$
	A4@A6B16	$Li_{13}Na_{29}Ba_{19}$
	A4@A10B12	$Cu_{23}Dy_6$, $Cu_{23}Tb_6$, $Cu_{23}Yb_6$
	A4@A12B10	$AgBe_2$, $AmFe_2$, $CaAl_2$
	A4@A16B6	Be_5Co, Be_5Pt, $CaAu_5$
	A4@A18B4	Be_5Co, Be_5Pt, $CaAu_5$
	A4@B4C6A12	$CaCu_4In$, $CaMgNi_4$, Cu_4MgIn
	A4@B4C18	$AuHf_{1.5}Al_{0.5}$, $AuZr_{1.5}Al_{0.5}$, $CuHf_{1.5}Zn_{0.5}$
γ-brass@16	A8@A24B10	$Cu_{41}Sn_{11}$
	A4B4@A34	$Sc_{44}Os_7$
	A4B4@A30B4	Ir_4Mg_{29}
	A4B4@A12B22	Au_9In_4, Ca_4Hg_9

Moreover, the $Au_{10}Cr_4Zn_{89}$ and $Au_{10}Mo_4Zn_{89}$ intermetallic compounds have the same combination of nanocluster models as they are isotypic. A closely related complex compound, β-$Al_{67.4}Cu_{14.3}Cr_{18.3}$, in the Al−Cu−Cr system crystallizes in space group $F\bar{4}3m$ (No. 216) having 412 atoms in its unit cell. The crystal structure of the newly synthesized compound, $Au_{10}Mo_4Zn_{89}$, and β-$Al_{67.4}Cu_{14.3}Cr_{18.3}$[54] have two similar two-cell nanoclusters. However, as a consequence of the disorder of β-$Al_{67.4}Cu_{14.3}Cr_{18.3}$, the 42-atom γ-brass-based nanocluster is not found (Table 5). Using the non-γ-brass description (see Figure 6), the combination of two 1@16@50 and □@6@28 primary nanoclusters and one 1@12 spacer is found in the superstructure of γ-brass-type (Fe,Ni)$Zn_{6.5}$.[55] This shows that the (Fe,Ni)$Zn_{6.5}$ and $Au_{10}Mo_4Zn_{89}$ structures have the same combination of nanocluster models. Moreover, in the (Fe,Ni)-$Zn_{6.5}$ structure, the three-shell @6@28@70 primary nanocluster is also identified. The Wyckoff positions of these crystal structures are similar, so they can be dominated by geometrical packing principles of nanoclusters.

An exact combination of three-shell nanoclusters is not seen in any intermetallic compounds; however, they can be found separately for some crystal structures of intermetallics. Looking for possible matching of the other three-shell nanoclusters, we found that the □@4@22@76 nanocluster is observed in the $Fe_{11}Zn_{40}$[56] and Ru_7Mg_{44}[57] structures as local configurations. The three-shell □@8@34@92 primary nanocluster has not been found in any intermetallic compounds beside that presented here.

In conclusion, it is important to note that an intermetallic structure cannot have only one universal nanocluster representation. This fact is the key point for finding an interesting relationship within the whole diversity of intermetallic compounds.

Electronic Structure Calculation. The refined ordered structure of $Au_{10}Mo_4Zn_{89}$ was used to perform electronic structure calculations to understand the stability of the compound. The DOS and COHP curves of $Au_{10}Mo_4Zn_{89}$ are shown in Figure 7. The overall shape of the total DOS curve is a parabola, which is the feature of free electron DOS, superimposed with a sharp peak located between −7 and −4 eV and a pronounced pseudogap at approximately −0.5 to 0.5 eV. The Fermi level for $Au_{10}Mo_4Zn_{89}$ falls into this pseudogap. In the COHP curves, E_F is located at (Au−Zn) or slightly below (Mo−Zn and Zn−Zn), the bonding−antibonding crossovers, indicating that the states are strongly bonding below the pseudogap, strongly antibonding above it, and nonbonding or weakly bonding and/or antibonding within it. All these characteristics above in DOS and COHP curves can also be observed in other γ-brass-type or related Hume−Rothery phases, offering us a rationalization for the composition−structure relationship of these phases. The compound can only be obtained with a VEC close to 1.67 per atom. It is noted that compound $MoZn_{20.44}$ represents the binary end point of the homogeneity range with no gold content. Assuming a rigid band approximation, the Fermi level for $MoZn_{20.44}$ (VEC = 1.72 e/a) is located at the upper limit of

dx.doi.org/10.1021/ic4013312 | Inorg. Chem. 2013, 52, 11110−11117

Table 5. Chemical Compositions of the Nanocluster Models of $Au_{10}M_4Zn_{89}$ (M = Cr and Mo) with the β-$Al_{67.4}Cu_{14.3}Cr_{18.3}$ and $(FeNi)_{.99}Zn_{12.71}$ Structures

structure	space group	Wyckoff position	nanocluster model	underlying net
$Au_{10}Mo_4Zn_{89}$	$F\bar{4}3m$	$h^5g^2fe^6b$	□@Zn_6@Mo_4Zn_{24} + □@Zn_4@Au_4Zn_{18} + □@Zn_8@Au_6Zn_{28} + Zn@Zn_{16}	bcu-x
$Au_{10}Cr_4Zn_{69}$		$h^5g^2fe^6b$	□@Zn_6@Cr_4Zn_{24} + □@Zn_4@Au_4Zn_{18} + □@Zn_8@Au_6Zn_{28} + Zn@Zn_{16}	bcu-xi
β-$Al_{67.4}Cu_{14.3}Cr_{18.3}$		$h^5gf^2e^6d$	□@Al_6@Cr_4Al_{24} + □@Al_4@Cr_4Al_{18} + □@Al_4@$Cr_{10}Al_{12}$ + Cu@$Cu_{12}Al_4$	bcu-x
$Au_{10}Mo_4Zn_{89}$		$h^5g^2fe^6b$	□@Zn_6@Mo_4Zn_{24} + Zn@Zn16@Zn46Mo4 + Zn@Zn10Au2	sqc349
(Fe,Ni)$Zn_{6.5}$		$h^5gf^2e^6da$	□@Zn_6@Fe_4Zn_{24} + Zn@Zn16@Zn42Fe8 + Zn@Zn11Fe1	sqc349

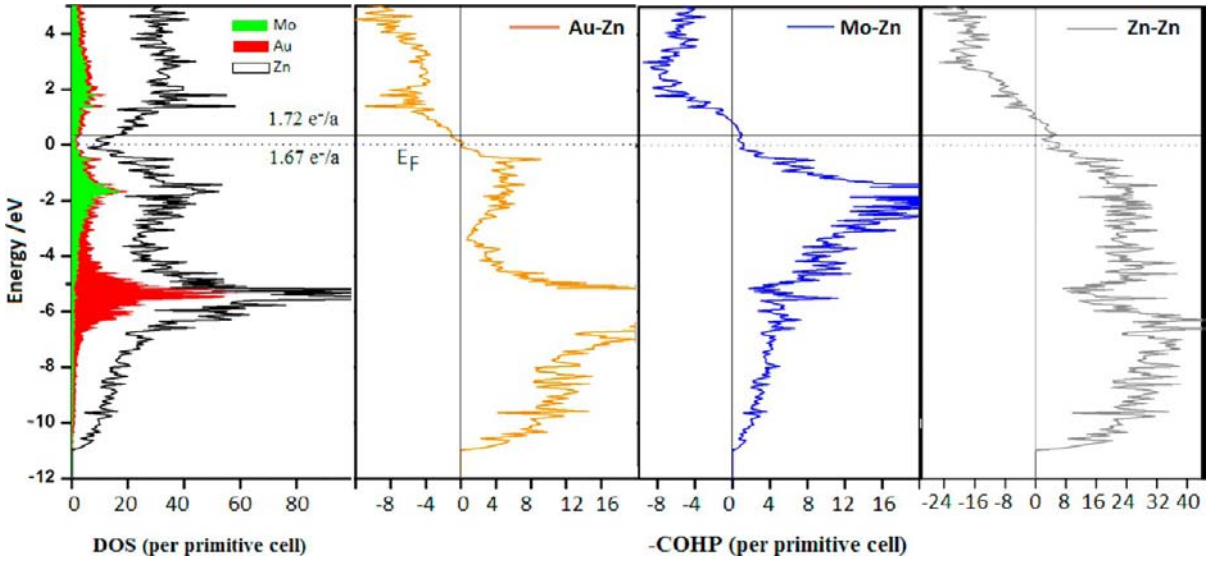

Figure 7. DOS and COHP curves of $Au_{10}Mo_4Zn_{89}$. The Fermi levels (E_F) for $MoZn_{20.44}$ and $Au_{10}Mo_4Zn_{89}$ are indicated by the solid black and dotted blue lines, respectively.

the pseudogap on this DOS curve indicated by a solid line. A significant deviation in VEC will either populate strongly antibonding states or depopulate strongly bonding states and thus destabilize the structure.

The contrast between Au 5d states and Mo 4d states is noteworthy. The Au 5d states are located between −7 and −4 eV, giving rise to the sharp peak in the DOS. They indeed interact with the Zn atoms in the icosahedron around Au, as indicated by the peak between −7 and −4 eV in the Au−Zn COHP curve. However, the fact that they are mainly concentrated within such a narrow energy range, significantly below the E_F, manifests their localized, semicore-state character. By contrast, Mo 4d states are higher in energy, spread over a much broader energy range (−4 to 3 eV), and split into two peaks separated by the pseudogap and E_F. The peak below the range of −4 to 0 eV corresponds to a strong bonding peak in the Mo−Zn COHP and the peak above the range of 0−3 eV to a strong antibonding peak. All these indicate that Mo 4d states are largely delocalized and actively bonded with the Zn atoms in the icosahedral coordination sphere.

CONCLUSION

The structure of $Au_{10}Mo_4Zn_{89}$ represents an ordered $2a \times 2a \times 2a$ superstructure of a γ-brass-related structure with 412 atoms in the cubic unit cell. The structure is isotypic to that of congeneric $Au_{10}Cr_4Zn_{89}$. A closer inspection of the atomic arrangements in $Au_{10}Mo_4Zn_{89}$ reveals that the cluster description may conveniently be expanded to 28-atom shells. In a nanocluster description, the model can be described as a combination of □@4@22, □@8@34, □@6@28, and 1@16 nanoclusters at positions: (0 0 0), ($^1/_4$ $^1/_4$ $^1/_4$), ($^3/_4$ $^3/_4$ $^3/_4$), and ($^1/_2$ $^1/_2$ $^1/_2$), respectively. The assembly of 34-atom (Ti_2Ni-based), 26-atom (γ-brass-type), and 42-atom (γ-brass-based) primary nanoclusters and a Friauf polyhedron (spacer) forms a **bcu-x** underlying net.

The valence electron concentration per atom is 1.67 for $Au_{10}Mo_4Zn_{89}$ and shows a pronounced pseudogap at the Fermi level.

Complex intermetallics arise through a delicate interplay between the chemical flexibilities of the individual elements. In γ-brass superstructures, there are typically two different interpenetrating networks that have subtly different geometric and electronic characteristics. Through Mulliken population analysis,[31] it is possible to derive a rationale for which sites should harbor the most electronegative element and which should be more electropositive. Intermediate sites tend to be those that are most affected by disorder. In the title compound, the introduction of a judiciously chosen third component, gold, that matches the constraints in terms of electron concentration, size, and electronegativity of the mixed sites in binary Mo−Zn obviates the need for mixed occupancy sites, and as a secondary effect, positional disorder also vanishes. We suggest that the mixed site occupancy of Mo/Zn may actually be seen as a pseudoelement that can be replicated by gold and that this principle may indeed be used to design new, ordered, ternary phases from disordered binary systems, or conversely novel ternary systems from known binaries.

dx.doi.org/10.1021/ic4013312 | Inorg. Chem. 2013, 52, 11110−11117

■ ASSOCIATED CONTENT

Supporting Information

EDS spectrum, structural data, X-ray crystallographic files in CIF file format, and an Excel file for the description of chemical compounds. This material is available free of charge via the Internet at http://pubs.acs.org.

■ AUTHOR INFORMATION

Corresponding Author

*E-mail: partha.jana@chem.lu.se.

Notes

The authors declare no competing financial interest.

■ ACKNOWLEDGMENTS

We are grateful to Dr. Fei Wang for his useful comments and suggestions on electronic structure calculations. We thank Prof. Vladislav A. Blatov and Davide M. Proserpio for their useful comments on nanocluster description. We thank the VR, Swedish National Science Council for the financial support. A.A.P. thanks the Russian Foundation for Basic Research (Grant 13-07-00001) and the Russian Government (Grant 14.B25.31.0005).

■ REFERENCES

(1) Hume-Rothery, W. *J. Inst. Met.* **1926**, *35*, 309.
(2) Hume-Rothery, W.; Raynor, G. V. *The Structure of Metals and Alloys*; Institute of Metal: London, 1954.
(3) Pearson, W. B. *The Crystal Chemistry and Physics of Metals and Alloys*; Wiley-Interscience: New York, 1972; pp 80−133.
(4) Pettifor, D. G. *Bonding and Structure of Molecules and Solids*; Oxford Science Publications: Oxford, U.K., 1995.
(5) Gourdon, O.; Gout, D. J.; Williams, J.; Proffen, T.; Hobbs, S.; Miller, G. J. *Inorg. Chem.* **2007**, *46*, 251−260.
(6) Brandon, J. K.; Brizard, R. Y.; Chieh, P. C.; McMillan, R. K.; Pearson, W. B. *Acta Crystallogr.* **1974**, *B30*, 1412−1417.
(7) van Heidenstam, O.; Johansson, A.; Westman, S. *Acta Chem. Scand.* **1968**, *22*, 653−661.
(8) Johansson, A.; Ljung, H.; Westman, S. *Acta Chem. Scand.* **1968**, *22*, 2743−2753.
(9) Gross, N.; Kotzyba, G.; Kunnen, B.; Jeitschko, W. *Z. Anorg. Allg. Chem.* **2001**, *627*, 155−163.
(10) Arnberg, L.; Westman, S. *Acta Chem. Scand.* **1972**, *26*, 513−517.
(11) Jana, P. P.; Lidin, S. *J. Solid State Chem.* **2013**, *201*, 244−249.
(12) Gourdon, O.; Miller, G. J. *Chem. Mater.* **2006**, *18*, 1848−1856.
(13) Gourdon, O.; Izaola, Z.; Elcoro, L.; Petricek, V.; Miller, G. J. *Philos. Mag.* **2006**, *86*, 419−425.
(14) Schmidt, J. T.; Lee, S.; Fredrickson, D. C.; Conrad, M.; Sun, J.; Harbrecht, B. *Chem.—Eur. J.* **2007**, *13*, 1394−1410.
(15) Morton, A. J. *Phys. Status Solidi A* **1974**, *23*, 275−289.
(16) Thimmaiah, S.; Conrad, M.; Lee, S.; Harbrecht, B. *Z. Anorg. Allg. Chem.* **2004**, *630*, 1762.
(17) Jana, P. P.; Lidin, S. *Eur. J. Inorg. Chem.* **2013**, *1*, 91−98.
(18) Jana, P. P.; Lidin, S. *Inorg. Chem.* **2012**, *51*, 9893−9901.
(19) Thimmaiah, S.; Miller, G. J. *Inorg. Chem.* **2013**, *52*, 1328−1337.
(20) Mahne, S.; Harbrecht, B. *J. Alloys Compd.* **1994**, *203*, 271−279.
(21) Jana, P. P.; Lidin, S. *CrystEngComm* **2013**, *15*, 745−753.
(22) Koster, A. S.; Schoone, J. C. *Acta Crystallogr.* **1981**, *B37*, 1905−1907.
(23) Nasch, T.; Jeitschko, W. *J. Solid State Chem.* **1999**, *143*, 95−103.
(24) Thimmaiah, S.; Richter, K. W.; Lee, S.; Harbrecht, B. *Solid State Sci.* **2003**, *5*, 1309−1317.
(25) Hornfeck, W.; Thimmaiah, S.; Lee, S.; Harbrecht, B. *Chem.—Eur. J.* **2004**, *10*, 4616−4626.
(26) Dshemuchadse, J.; Jung, D. Y.; Steurer, W. *Acta Crystallogr.* **2011**, *B67*, 269−292.
(27) Lidin, S.; Jacob, M.; Larsson, A.-K. *Acta Crystallogr.* **1994**, *C50*, 340−342.
(28) Pavlyuk, V.; Solokha, P.; Zelinska, O.; Paul-Boncour, V.; NowikZajac, A. *Acta Crystallogr.* **2008**, *C64*, i50−i52.
(29) Thimmaiah, S.; Crumpton, N. A.; Miller, G. J. *Z. Anorg. Allg. Chem.* **2011**, *637*, 1992−1999.
(30) Thimmaiah, S.; Miller, G. J. *Chem.—Eur. J.* **2010**, *16*, 5461−5471.
(31) Jana, P. P.; Henderson, R.; Harbrecht, B.; Lidin, S. *Inorg. Chem.* **2013**, *52*, 4812−4818.
(32) Lin, Q.; Corbett, J. D. *Inorg. Chem.* **2004**, *43*, 1912−1919.
(33) Petricek, V.; Dusek, M.; Palatinus, L. *The Crystallographic Computing System. Jana 2006*; Institute of Physics: Praha, Czech Republic, 2006.
(34) Palatinus, L.; Chapuis, G. *J. Appl. Crystallogr.* **2007**, *40*, 786−790.
(35) Blatov, V. A. *Struct. Chem.* **2012**, *23*, 955−963.
(36) Blatov, V.; Ilyushin, G. D.; Proserpio, D. M. *Inorg. Chem.* **2010**, *49*, 1811−1818.
(37) Andersen, O. K. *Phys. Rev. B* **1975**, *12*, 3060−3083.
(38) Andersen, O. K.; Jepsen, O. *Phys. Rev. Lett.* **1984**, *53*, 2571−2574.
(39) Andersen, O. K.; Jepsen, O.; Glötzel, D.; Lambrecht, W. R. L. In *Highlights of Condensed Matter Theory*; Bassani, F., Fumi, F., Tosi, M. P., Eds.; North-Holland: New York, 1985.
(40) Andersen, O. K. *Phys. Rev. B* **1986**, *34*, 2439−2449.
(41) von Barth, U.; Hedin, L. *J. Phys. C* **1972**, *5*, 1629−1642.
(42) Koelling, D.; Harmon, B. N. *J. Phys. C* **1977**, *10*, 3107−3114.
(43) Jepsen, O.; Andersen, O. K. *Z. Phys. B* **1995**, *97*, 35−47.
(44) Blçchl, P. E.; Jepsen, O.; Andersen, O. K. *Phys. Rev. B* **1994**, *49*, 16223−16233.
(45) Chabot, B.; Cenzual, K.; Parthé, E. *Acta Crystallogr.* **1981**, *A37*, 6−11.
(46) Hellner, E.; Koch, E. *Acta Crystallogr.* **1981**, *A37*, 1−6.
(47) Nowotny, H.; Bauer, E.; Stempfl, A. *Monatsh. Chem.* **1950**, *81*, 679−680.
(48) Lord, E. A.; Ranganathan, S. *J. Non-Cryst. Solids* **2004**, *334*−*335*, 121−125.
(49) Frank, F. C.; Kasper, J. S. *Acta Crystallogr.* **1958**, *11*, 184−190.
(50) Alvarez, S. *Dalton Trans.* **2006**, *17*, 2045−2051.
(51) Kreiner, G.; Franzen, H. F. *J. Alloys Compd.* **1995**, *221*, 15−36.
(52) O'Keeffe, M.; Peskov, M. A.; Ramsden, S. J.; Yaghi, O. M. *Acc. Chem. Res.* **2008**, *41*, 1782−1789.
(53) Pankova, A. A.; Blatov, V. A.; Ilyushin, G. D.; Proserpio, D. M. *γ*-Brass polyhedral core in intermetallics: The nanocluster model, manuscript in preparation.
(54) Sugiyama, K.; Saito, H.; Hiraga, K. *J. Alloys Compd.* **2002**, *342*, 148−152.
(55) Lidin, S.; Jacob, M.; Larsson, A. K. *Acta Crystallogr.* **1994**, *C50*, 340−343.
(56) Koster, A. S.; Schoone, J. C. *Acta Crystallogr.* **1981**, *B37*, 1905−1907.
(57) Westin, L.; Edshammar, L.-E. *Chem. Scr.* **1973**, *3*, 15−22.